Correspondence

A High-Tolerance Matching Method Against Load Fluctuation for Ultrasonic Transducers

Jin-Dong Wang, Jia-Jia Jiang, *Member, IEEE*, Fa-Jie Duan, Shuo-Ya Cheng, Cheng-Xiang Peng, Wei Liu, *Senior Member, IEEE*, and Xing-Hua Qu

***Abstract*—Fluctuation of acoustic load significantly weakens the performance of ultrasonic system. To address this problem in a simple way, we consider the main input and output variables related to the ultrasonic transducer's performance and propose a detailed mathematical model based on the simplest *LC* matching network containing only one capacitor and one inductor. In this model, a new resonance frequency f_0 brought by matching components was found and defined. The optimum analysis method is used to solve the model, and a high-tolerance matching method against load fluctuation is obtained. Analysis indicates that when activated at the mechanical resonance frequency, the impedance and apparent power of the piezoelectric transducer (PT) matched by the proposed method are constant no matter how the load changes, and thereby can significantly increase the stability and robustness of ultrasonic systems. For its simple structure and high performance, the proposed matching method can be widely applied in most ultrasonic systems. The tolerance of the proposed method against other environmental factors and high-order *LC* matching networks were also discussed. In addition, the feasibility and advantage of the proposed matching method are also verified by experiments.**

***Index Terms*—Matching circuit, matching network, power ultrasound, ultrasonic power supply, ultrasonic processing, ultrasonic transducer.**

I. Introduction

Over the past decades, power ultrasound has been widely used in industry [1], in ultrasonic welding [2], [3], ultrasonic motor [4], [5], ultrasonic cleaning [6], and ultrasonic manufacturing [7]–[10], etc. As a key component of ultrasonic systems, an ultrasonic piezoelectric transducer (PT) connects driving power supply and load, transfers the electrical energy into a high-frequency vibration, and then transfers it to the other vibration systems [11].

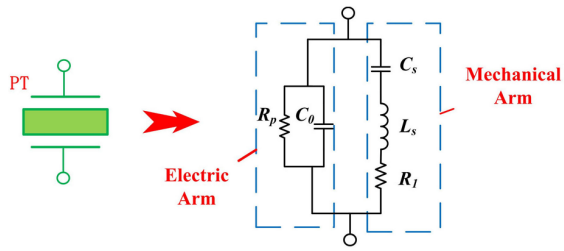

Fig. 1. Equivalent circuit model of a PT which consists of two arms.

As illustrated in Fig. 1, a PT can be modeled as a simple circuit [11], [12] that consists of two arms: one is the electric arm, including a static capacitor C_0 and a dielectric loss resistance R_p, and the other is the mechanical arm, including a dynamic capacitor C_s, a dynamic inductor L_s, and a mechanical loss resistance R_1. The value of R_1 reflects the degree of acoustic load. Since R_p is much bigger than R_1, it is often ignored in calculations [13]. Besides, when a mechanical resonance happens, L_s and C_s will cancel out each other so that the PT reaches the best performance [14]. The mechanical resonance frequency f_s, whose corresponding angular frequency is ω_s, can be calculated by

$$f_s = 1/(2\pi\sqrt{L_s C_s}). \tag{1}$$

However, due to the existence of C_0 the equivalent circuit of a PT is capacitive at f_s, which reduces energy efficiency [14], [15]. Special circuits, the so-called inductor–capacitor (*LC*) matching networks [16]–[22], which are made up of capacitors and inductors are often applied to remove the negative effect of C_0. The simplest *LC* matching network is shown in Fig. 2(a), wherein it can be seen that it consists of only one capacitor and one inductor, where L is the matching inductor, C_2 is the matching capacitor, and V_{in} is the voltage of driving signal whose angular frequency is ω_{dr}. Defining C as the sum of C_2 and C_0, the circuit can be further simplified as shown in Fig. 2(b). Taking this circuit as an example, when the mechanical resonance happens, i.e., at $\omega_{dr} = \omega_s$, then the equivalent circuit can be illustrated as displayed in Fig. 2(c). The complex impedance $Z(\omega_s)$ in Fig. 2(c) can be expressed as follows:

$$Z(\omega_s) = j\omega_s L + \left(R_1 - j\omega_s {R_1}^2 C\right) / \left(1 + {\omega_s}^2 {R_1}^2 C^2\right). \tag{2}$$

To make the equivalent circuit become a pure-resistance circuit, the imaginary part of $Z(\omega_s)$ should be zero. Thus, the values of L and C

Manuscript received January 18, 2019; revised April 25, 2019; accepted June 1, 2019. Date of publication June 5, 2019; date of current version October 18, 2019. This work was supported in part by the Tianjin Natural Science Foundations of China under Grant 17JCQNJC01100, in part by the National Natural Science Foundations of China under Grants 61501319 and 51775377, in part by the National Key Research and Development Plan under Grant 2017YFF0204800, in part by the Young Elite Scientists Sponsorship Program By Cast of China under Grant 2016QNRC001, in part by the Key Technologies R&D program of Tianjin under Grant18YFZCGX00920, and in part by the National Key R&D Program of China under Grant 2018YFF0212702. Recommended for publication by Associate Editor J. Popovic-Gerber. *(Jin-Dong Wang and Jia-Jia Jiang contributed equally to this work.) (Corresponding author: Fa-Jie Duan.)*

J.-D. Wang, J.-J. Jiang, F.-J. Duan, and X.-H. Qu are with the State Key Lab of Precision Measuring Technology & Instruments, Tianjin University, Tianjin 300072, China (e-mail: tju_jdwang@163.com; jiajiajiang@tju.edu.cn; fjduan@tju.edu.cn; quxinghua@tju.edu.cn).

S.-Y. Cheng is with the School of Electrical and Information Engineering, Tianjin University, Tianjin 300072, China (e-mail: shuoya@tju.edu.cn).

C.-X. Peng is with the Beijing Institute of Space Mechanics and Electricity, Beijing 100094, China (e-mail: pengcx@tju.edu.cn).

W. Liu is with the Department of Electronic and Electrical Engineering, University of Sheffield, Sheffield, S1 3JD, U.K. (e-mail: w.liu@sheffield.ac.uk).

Color versions of one or more of the figures in this paper are available online at http://ieeexplore.ieee.org.

Digital Object Identifier 10.1109/TPEL.2019.2921384

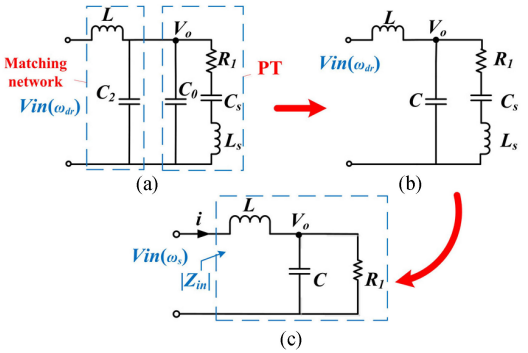

Fig. 2. (a) Equivalent circuit model of a PT after *LC* matching, (b) simplified circuit, and (c) simplified circuit when mechanical resonance happens.

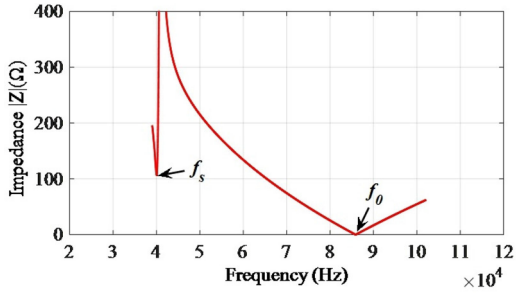

Fig. 3. Impedance-frequency curve after *LC* matching, a new resonance frequency f_0 is brought in, where $R_1 = 200.96\ \Omega$, $C_s = 0.276$ nF, $L_s = 56.54$ mH, $C_2 = C_0 = 5.24$ nF, and $L = 32.97$ mH.

should satisfy the following relationship:

$$L = {R_1}^2 C / \left(1 + {\omega_s}^2 {R_1}^2 C^2\right). \tag{3}$$

The piezoelectric transducers usually have high electric quality factors, and their resonance frequency often changes with environmental parameters such as temperature, humidification, and others [23], [24]. Meanwhile, R_1 varies dramatically from several ohms under no-load conditions to hundreds of ohms or more under heavy-load conditions [25]. According to (3), the matching will fail when the piezoelectric transducer's resonance frequency f_s or acoustic load R_1 changes [22], [26], which denote the two main problems affecting the output stability of an ultrasonic system. Nevertheless, the output stability is one of the most paramount performance indicators that have a significant effect on cleaning, welding, and machining results [7], [27]. The transient response is also crucial to the power system performance. Besides, a surge current can cause system damage and overpower output can destroy the operating objects.

To address the first mentioned problem, many resonance frequency tracking (RFT) methods have been proposed [13], [14], [23]–[25], [27]–[33], and the accuracy of RFT methods has been continuously improving. As for the second mentioned problem, generally, there are two ways to solve it. One is by using the feedback control systems [15], [27]–[30], [34] that maintain a constant output power or amplitude by a closed-loop (adaptive) voltage or current scaling [4]. The other is by adding the adjustable components [5], [22], [35]. Although both these ways are effective, they can solve the load fluctuation problem only to a certain extent. Also, the operating range is limited by their high cost, slow response time, and relatively low stability. In [36], an adjustable inductor array was used to achieve the adaptive matching of load change. However, this solution includes a large number of components which is not suitable for high-power applications. Besides, in the matching network design, the goal is mainly to achieve the broadband driving [6] or to improve the transmitting efficiency [17], [18], [21], [37], [38], by comparison, few are aimed to improve the tolerance against load fluctuation.

Different from the aforementioned solutions, improving the tolerance against the load fluctuation is considered as the primary design objective in this paper. We aim to achieve a stable, high-performance matching result and solve the second problem using the simplest *LC* matching network, which is shown in Fig. 2(a). Although there are many studies or schemes concerning *LC* matching networks, the optimal values for the matching components have not been given yet.

In this paper, we first conduct a careful analysis of the variables related to the input and output signals of an ultrasonic system, and then we develop a mathematical model based on the matching network that is displayed in Fig. 2(a). A resonance frequency of the newly formed circuit, wherein the matching components are added, is found and defined to help solving the model. By using the optimum analysis method, a high-tolerance matching method against load fluctuation is developed. The conducted analysis shows that the transducer matched by the proposed method has excellent electrical properties which can be summarized as follows:

1) At the mechanical resonance frequency, the impedance $|Z_{\rm in}|$ of the circuit is constant regardless of the load changes, so that the current i and the apparent power S are also constant.

2) The transducer's output power P is the most stable and reaches the maximum at a typical load.

3) Under the transient conditions, the current and output power of a system do not rise dramatically, thus protecting the system and operating objects.

This paper is organized as follows. Section II details the derivation process of the proposed method. Section III discusses the sensitivity of the proposed method and explores the possibilities of high-order matching networks. In Section IV, experiments are carried out using an ultrasonic driving and control system to verify the performance of the proposed matching method, and Section V provides a conclusion.

II. Modeling Analysis and the Proposed Method

Modeling is the bridge to solve various practical problems by mathematical methods. The detailed modeling process includes determining variables and their relationships, modeling, model solving, and model evaluation. In this paper, the matching network shown in Fig. 2(a) with one capacitor and one inductor is our primary modeling focus.

A. Variables Determination

Generally, the final output of an ultrasonic system is high-frequency power ultrasound consisted of the active power P and the apparent power S. The former denotes the actual output power, and the latter denotes the power the system undertakes. Some of the relevant-dependent variables are the impedance $|Z|$ and power factor μ.

After matching, the impedance-frequency curve of the circuit shown in Fig. 2(a) is as illustrated in Fig. 3. Fig. 3 shows that a new resonance frequency is newly brought by the matching inductor and capacitor. We named it as the *LC* resonance frequency f_{LC}, and it is expressed as follows:

$$f_{LC} = 1/2\pi\sqrt{LC}. \tag{4}$$

Note that f_{LC} is a very critical frequency for the circuit because, at that frequency, the impedance is zero so that adding even a small

amount of power can cause circuit damage. Therefore, the value of f_{LC} must be taken into account when selecting matching parameters.

In practice, the RFT algorithms track the real-time frequency of f_s, but the difference between the frequency f_{dr} of driving voltage and actual resonance frequency f_s is unavoidable. Furthermore, there are also errors in calculating the matching parameters by using (3). Suppose the actual values of f_s and R_1 in (3) are f_{ma} (the corresponding angular frequency is ω_{ma}) and R_0, where R_0 denotes the load resistance under typical working condition. R_0 can be selected according to the actual conditions.

To demonstrate how the above-mentioned errors affect the matching results, we define several new variables as follows:

$$\rho = f_s/f_{LC} \tag{5}$$

$$\rho_1 = f_{dr}/f_s \tag{6}$$

$$\rho_2 = f_{ma}/f_s \tag{7}$$

$$\rho_3 = R_1/R_0 \tag{8}$$

where ρ denotes the ratio of f_s to f_{LC}, we denoted it as a matching parameter, ρ_1 represents the error of resonance frequency tracking, ρ_2 represents the change in matching inductor L and capacitor C, and ρ_3 represents the fluctuation of acoustic load R_1.

The values of L and C are constrained by (3) and (4), so when ρ is determined, the values of L and C are unique. By using (3)–(5), the values of L and C can be respectively obtained by

$$L = \rho\sqrt{{\omega_s}^2 - \rho^2{\omega_{ma}}^2}R_0/{\omega_s}^2 = \rho\sqrt{1-\rho^2{\rho_1}^2}R_0/\omega_s \tag{9}$$

$$C = \rho/\left(\sqrt{{\omega_s}^2 - \rho^2{\omega_{ma}}^2}R_0\right) = \rho/\left(\sqrt{1-\rho^2{\rho_1}^2}\omega_s R_0\right). \tag{10}$$

Meanwhile, according to (3)–(5), the value range of ρ is limited by C, and ρ can be expressed by

$$\rho = \frac{f_s}{f_{LC}} = \frac{\omega_s}{\omega_{LC}} = \omega_s\sqrt{LC} = \frac{\omega_s R_1}{\sqrt{1/C^2 + {\omega_s}^2{R_1}^2}}. \tag{11}$$

Equation (11) shows that ρ reaches the maximum value of 1 when C is infinitely large, and it reaches the minimum value when $C = C_0$. Thus, the value range of ρ is defined as $\left(\frac{\omega_s R_1}{\sqrt{\frac{1}{C_0^2}+\omega_s^2 R_1^2}},\ 1\right)$.

Another crucial parameter of a PT is the mechanical quality factor Q_m, which is defined by

$$Q_m = \sqrt{L_s/C_s}/R_1 = 1/\omega_s R_1 C_s. \tag{12}$$

According to (1) and (12), L_s and C_s can be expressed in terms of R_1, Q_m, and f_s, as follows:

$$C_s = 1/Q_m\rho_3 R_0\omega_s,\ L_s = Q_m\rho_3 R_0/\omega_s. \tag{13}$$

B. Modeling of the Matched Circuit

Modeling of the matched circuit is carried out under two basic assumptions given in the following. 1) The equivalent circuit model of a PT after *LC* matching is as presented in Fig. 2(b), wherein all the inductors, capacitors, and resistances are ideal. 2) The driving voltage $v_{\rm in}$ can be approximated by a sinusoidal waveform with the frequency f_{dr}, i.e. $v_{\rm in} = V_{\rm in}\sin(2\pi f_{dr}t)$.

In Fig. 2(b), the total complex impedance $Z_{\rm in}$ can be expressed by

$$Z_{\rm in} = j\omega_{dr}L + \frac{1}{j\omega_{dr}C}\Big\|\left(R_1 + \frac{1}{j\omega_{dr}C_s} + j\omega_{dr}L_s\right). \tag{14}$$

According to (5)–(13), (14) can be further rewritten as follows:

$$Z_{\rm in} = j\rho_2\rho\sqrt{1-\rho^2{\rho_1}^2}R_0 + \frac{\sqrt{1-\rho^2{\rho_1}^2}R_0}{j\rho\rho_2}\Big\|\left(\rho_3 R_0 + \frac{Q_m\rho_3 R_0}{j\rho_2} + j\rho_2 Q_m\rho_3 R_0\right). \tag{15}$$

The apparent power S, the power factor μ, and the total active power P of an ultrasonic system can be respectively calculated by

$$S = {V_{\rm in}}^2/|Z_{\rm in}| \tag{16}$$

$$\mu = \mathrm{real}(\mathrm{Z_{in}})/|\mathrm{Z_{in}}| \tag{17}$$

$$P = S\cdot\mu = {V_{\rm in}}^2\mathrm{real}\left(Z_{\rm in}\right)/|Z_{\rm in}|^2. \tag{18}$$

The output power of an ultrasonic system represents the power obtained by mechanical loss resistance R_1. Since R_1 is the only active component of the PT, the total active power P is the actual output power of the circuit. Furthermore, the model can be defined as follows:

$$(Z_{\rm in}, Q_m, P, \mu) = f\left(\rho, \rho_1, \rho_2, \rho_3\right) \tag{19}$$

where f is illustrated in (15)–(18), ρ indicates the matching parameter to be determined, and ρ_1, ρ_2, and ρ_3 are the input variables.

C. Model Solving

The load's fluctuation is taken as the main influence factor for the circuit's performance, so the RFT error is ignored first, i.e., $\rho_2 = 1$; meanwhile, ρ_1 is equal to 1 too. And ρ_2 and ρ_1 will be used in validating the feasibility of the proposed method.

Substituting $\rho_2 = 1$ and $\rho_1 = 1$ into (15), $Z_{\rm in}$ can be further expressed by

$$Z_{\rm in} = j\left[\rho\sqrt{1-\rho^2}R_0 - \frac{{\rho_3}^2\rho\sqrt{1-\rho^2}R_0}{1-\rho^2+\rho^2{\rho_3}^2}\right] + \frac{\rho_3\left(1-\rho^2\right)R_0}{1-\rho^2+\rho^2{\rho_3}^2}. \tag{20}$$

The impedance $|Z_{\rm in}|$ can be deduced as follows:

$$|Z_{in}| = \left(1-\rho^2\right)R_0\sqrt{\frac{{\rho_3}^2+\rho^2-\rho^2{\rho_3}^2}{1-\rho^2+\rho^2{\rho_3}^2}}. \tag{21}$$

The real part of $Z_{\rm in}$, $\mathrm{real}(Z_{\rm in})$ is defined by

$$\mathrm{real}\left(Z_{\rm in}\right) = \frac{\rho_3\left(1-\rho^2\right)R_0}{1-\rho^2+\rho^2{\rho_3}^2}. \tag{22}$$

By substituting (21) and (22) into (16)–(18), we obtain

$$S\left(\rho,1,1,\rho_3\right) = {V_{\rm in}}^2\Big/\left[\left(1-\rho^2\right)R_0\sqrt{\frac{{\rho_3}^2+\rho^2-\rho^2{\rho_3}^2}{1-\rho^2+\rho^2{\rho_3}^2}}\right] \tag{23}$$

$$\mu\left(\rho,1,1,\rho_3\right) = 1/\sqrt{\left(1-\rho^2+\rho^2/{\rho_3}^2\right)}\left(1-\rho^2+\rho^2{\rho_3}^2\right) \tag{24}$$

$$P\left(\rho,1,1,\rho_3\right) = \frac{{V_{\rm in}}^2}{\left(1-\rho^2\right)R_0\left[\left(1-\rho^2\right)\rho_3+\rho^2/\rho_3\right]}. \tag{25}$$

Under typical load, i.e., $R_1 = R_0$, $\rho_3 = 1$, and the typical value of S and P are given

$$S\left(\rho,1,1,1\right) = {V_{\rm in}}^2/\left[\left(1-\rho^2\right)R_0\right] \tag{26}$$

$$P\left(\rho,1,1,1\right) = {V_0}^2/R_1 = {V_{\rm in}}^2/\left[\left(1-\rho^2\right)R_0\right]. \tag{27}$$

To express the change in the values of S and P, we define α_1 as the ratio of the actual apparent $S(\rho,1,1,\rho_3)$ power to the typical apparent power $S(\rho,1,1,1)$, and α_2 as the ratio of the actual active power $P(\rho,1,1,\rho_3)$ to the typical active power $P(\rho,1,1,1)$

$$\alpha_1 = \frac{S(\rho,1,1,\rho_3)}{S(\rho,1,1,1)} = 1\Big/\sqrt{\frac{1}{(1-2\rho^2)/(\rho_3{}^2+1)+\rho^2}-1} \quad (28)$$

$$\alpha_2 = \frac{P(\rho,1,1,\rho_3)}{P(\rho,1,1,1)} = \frac{1}{(1-\rho^2)\rho_3+\rho^2/\rho_3} = \frac{1}{\rho_3+1/(\rho_3-\rho_3)\rho^2}. \quad (29)$$

With the aim to reduce the impact of the fluctuant load on the output power as much as possible, both α_1 and α_2 should be as close as possible to 1. Based on (28), at $\rho = 1/\sqrt{2}$, α_1 is equal to 1, which indicates the apparent power is always constant under variable-load conditions; thus, it can be written that

$$S\left(1/\sqrt{2},1,1,1\right) = {V_{\rm in}}^2/\left[\left(1-\rho^2\right)R_0\right] = 2{V_{\rm in}}^2/R_0. \quad (30)$$

Accordingly, $1/\sqrt{2}$ is taken as a candidate value of ρ. Based on (29), α_2 is positively correlated to ρ when $\rho_3 > 1$, and negatively correlated to ρ when $\rho_3 < 1$. This means it is contradictory in the two conditions, $\rho_3 > 1$ and $\rho_3 < 1$, when selecting the value of ρ, so a compromised method is needed. Hence, for the denominator of (25), we have

$$\left(1-\rho^2\right)R_0\left[\left(1-\rho^2\right)\rho_3+\rho^2/\rho_3\right] \geq 2\rho\left(1-\rho^2\right)^{\frac{3}{2}}R_0. \quad (31)$$

Therefore, a maximum value $P_{\max}$ exists, and it is given by

$$P_{\max} = \frac{{V_{\rm in}}^2}{2\rho(1-\rho^2)^{\frac{3}{2}}R_0}. \quad (32)$$

When P is max, we obtain the following:

$$\rho_{3\max P} = \rho/\sqrt{1-\rho^2}. \quad (33)$$

In general, the transducer is expected to reach the maximum power at the typical load so as to improve its power efficiency. Thus, the active power could reach the maximum value at $\rho_3 = 1$. Applying $\rho_3 = 1$ to (33), we obtain the following:

$$\rho = 1/\sqrt{2}. \quad (34)$$

The obtained value is the same as the above candidate value, so we have

$$\alpha_2 = \frac{2}{1/\rho_3+\rho_3}. \quad (35)$$

Equation (35) indicates that the active power has the same changing trend both when the load increases and decreases. Substituting $\rho = 1/\sqrt{2}$ to (21), the impedance is obtained as follows:

$$\left|Z_{\rm in}\left(1/\sqrt{2},1,1,\rho_3\right)\right| = \frac{R_0}{2}\sqrt{\frac{{\rho_3}^2+1/2-{\rho_3}^2/2}{1-1/2+{\rho_3}^2/2}} = \frac{R_0}{2}. \quad (36)$$

According to (30), (35), and (36), at $\rho = 1/\sqrt{2}$, the impedance and apparent power are constant under variable load; thus, the current of the main loop does not change either. Besides, according to (35), at $\rho = 1/\sqrt{2}$, the active power P has the least fluctuation and achieves the maximum value at the typical load. Therefore, the system tolerance of load fluctuation can be improved. Thus, $\rho = 1/\sqrt{2}$ is adopted as an optimum value in the solution of the proposed model. Substituting $\rho = 1/\sqrt{2}$ into (9) and (10), the optimal values of matching inductor and capacitor can be respectively calculated by

$$L = R_0/(2\omega_s), C = 1/(\omega_s R_0) \quad (37)$$

$$C_2 = C - C_0 = 1/(\omega_s R_0) - C_0. \quad (38)$$

Moreover, a schematic diagram is provided to help understanding the model, as shown in Fig. 4(a).

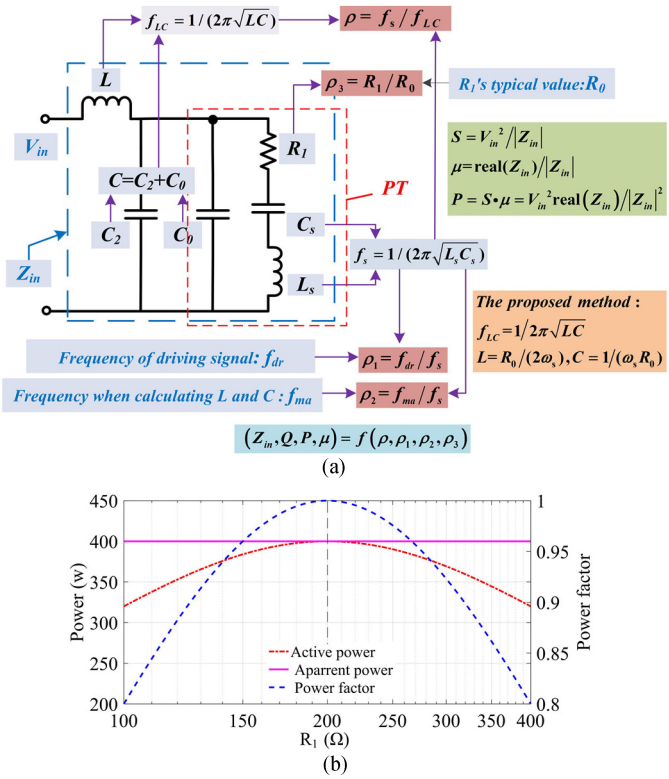

Fig. 4. (a) Schematic diagram of the built model. (b) Power-load curves of the proposed method.

D. Modeling Results Evaluation

Considering the minimum power fluctuation as the main objective, we derive the optimum values of matching components based on the developed model. The optimal values of matching inductor and capacitor are given in (37) and (38).

To describe the actual effect of the model solution results more intuitively, a virtual PT's power response over the load value is calculated by (23)–(25), using the following parameters: $C_0 = 4.97$ nF, $L_s = 39.7$ mH, $C_s = 0.401$ nF (hence, $f_s = 40056$ Hz), and the typical mechanical loss resistance R_0 is 200 Ω. The voltage of driving signal $V_{\rm in} = 200$ V. Using (30), both the typical apparent power and active power are calculated to 400 W. Using (37) and (38), we have $L = 0.3973$ mH and $C = 19.867$ nF. Supposing the loss resistance R_1 varies from 140 to 300 Ω, and the frequency of driving signal is $f_{dr} = f_s = 40056$ Hz, then the power-load curves are as shown in Fig. 4(b). Besides, using to (15)–(18), the power-load curves in other cases ($\rho = 1/4, 1/3, 1/2, 1/\sqrt{3}, 1/\sqrt{2}$, and $4/5$) are also calculated, and they are depicted in Fig. 5 where it can be seen that the virtual transducer performs much better at $\rho = 1/\sqrt{2}$ than the other conditions. The excellent characteristics at $\rho = 1/\sqrt{2} =$ can be summarized as follows.

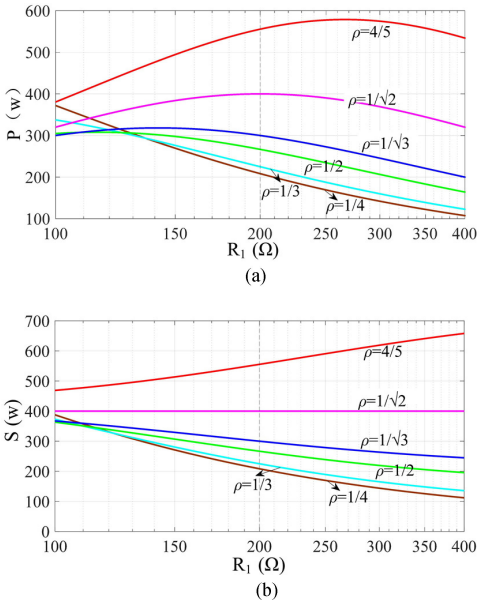

Fig. 5. Power-load curves of a virtual PT with different value of ρ. (a) Active power change curves over load. (b) Apparent power change curves over load.

1) The active power P reaches the maximum value of 400 W under the typical load of 200 Ω, and at that load value, the active power fluctuates the least.
2) The apparent power S is an absolute constant regardless of the changing trend of load R_1, and the current flowing through the whole system is constant too; thus, the transient impact can be well restrained which ensures system safety.

Note that all the results were obtained by the simulations in the MATLAB R2016b simulation platform.

III. Sensitivity Analysis and High-Order *LC* Matching Networks

The excellent characteristics of the proposed method are presented in Section II. However, the above analysis is based on the assumption that errors of both RTF and matching frequency are zero ($\rho_2 = 1$, $\rho_1 = 1$), which is impossible in practice, where the change in environmental parameters, such as temperature, causes the change in values of capacitance and inductance. Accordingly, it is necessary to discuss the feasibility of the proposed method when ρ_1 and ρ_2 differ from 1. This analysis is also known as a sensitivity analysis.

Additionally, a kind of high-order *LC* matching network with special characteristics is provided which in some cases can provide more possibilities or better performances.

A. Sensitivity Analysis of the Proposed Method

The environmental factors cause a change in the values of f_s and matching components, thereby f_{dr} is no longer equal to f_s. The RFT algorithms can be used to track f_s. Also, the error between f_s and f_{ma} cannot be ignored. The driving frequency error Δf and the matching frequency error Δf_1 are respectively defined by

$$\Delta f = f_{dr} - f_s \tag{39}$$

$$\Delta f_1 = f_{ma} - f_s \tag{40}$$

where Δf depends on the accuracy of the RTF algorithm, and Δf_1 is decided by the shift of f_s and the error of matching components. Generally, the value of Δf is tens Hz or less, while the value of Δf_1 is hundreds or thousands. To demonstrate the impact of Δf and Δf_1 on the model, the simulations were performed on the same virtual PT as that used in Section II-D. The results are shown in Figs. 6 and 7, wherein Δf is in the range from –150 to 150 Hz, Δf_1 is in the range from –2000 to 2000 Hz, and R_1 is in the range from 100 to 300 Ω. Using (30), both the typical apparent power and active power were calculated to be 400 W.

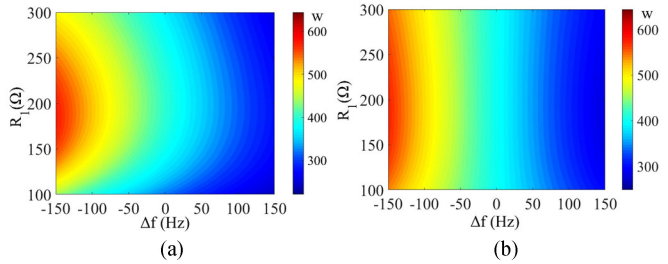

Fig. 6. Effects of Δf on the output power of the ultrasonic system matching by the proposed method. (a) Active power. (b) Apparent power.

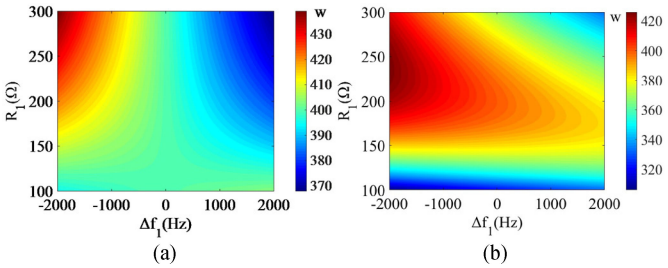

Fig. 7. Effects of Δf_1 on the output power of the ultrasonic system matching by the proposed method. (a) Active power. (b) Apparent power.

As shown in Figs. 6 and 7, the output power was more sensitive to Δf than Δf_1. When Δf was zero, the apparent power was constant (0%), and the active power varied within 60 W (–15%–0%). When the RTF error was within ±40 Hz, the maximum fluctuation ranges of the apparent power and active power were from 320 to 450 W (–20%–+12.5%). However, when Δf was greater than 100 Hz, the maximal output power difference was almost 300 W (+75%), which indicates that when the driving frequency varied largely, the matching was invalid. Fortunately, most RFT algorithms can provide an accuracy of ±40 Hz or higher [13], [14], [25].

On the other hand, Δf_1 had a little effect on the output power (less than 15%) in a very wide range (±1 kHz). In practice, the stability of the matching inductor and capacitor is better than 1%, and the variation of f_s is less than 500 Hz; thus, the value of Δf_1 is rarely above 1 kHz even under extreme conditions.

In conclusion, the simulation results indicate that even though the proposed matching method is influenced by the fluctuations in environmental conditions and RFT error, it is still valid in most conditions.

B. High-Order LC Matching Networks

Among various network topologies, two kinds of high-order *LC* matching networks [39], which are also known as multistage L-section matching networks, are typically the most efficient, and they are shown in Fig. 8. The second kind of circuit shown in Fig. 8(b), which is suitable for stepping-up voltage, is discussed in this paper.

As shown in Fig. 8(b), the relationship between Z_n and Z_{n-1} can be expressed as follows:

$$Z_n = 1/\left(1/Z_{n-1} + j\omega C_n\right) + j\omega L_n. \tag{41}$$

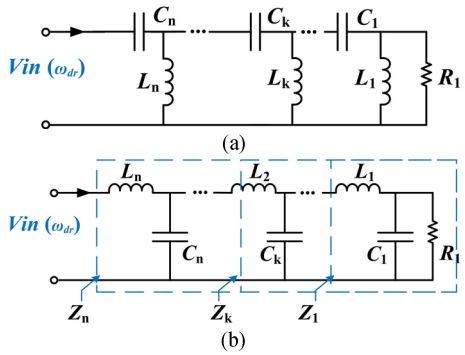

Fig. 8. Two kinds of high-order matching networks. (a) Stepping-up current. (b) Stepping-up voltage.

Considering the condition that the ultrasonic system is under the typically load, i.e., $R_1 = R_0$, to achieve similar functionality as the proposed one-order matching method, we can get $Z_1 = R_0/2$, $Z_2 = R_0/2^2$, according to (36), and by analogy $Z_k = R_0/2^k$ $(k = 1, 2 \ldots, n)$. Accordingly, the values of L_k and C_k in Fig. 8(b) could be determined by (37)

$$L_k = R_0/(2^k \omega_s), C_k = 2^{k-1}/(\omega_s R_0). \tag{42}$$

Substituting (42) and (41) into (16)–(18), and using the same parameters as in part A, the power$/2^{n-1}$-*load* curves (including *S* and *P*) and the *power factor-load* curves, for different n, are depicted in Fig. 9. In Fig. 9, it can be seen that the curves are all periodic and have excellent properties. For the power$/2^{n-1}$-*load* curves, the cycle value is 4, and when n is odd, the curves have the same shape with the one-order network, i.e., S is constant. More significantly, Fig. 9(c) reveals a new excellent feature of the circuit presented in Fig. 8(b), that is, when n is even, the system power factor is always constant and equal to 1. We name the special circuit shown in Fig. 8(b) [with the components' values given by (42)] the *Wang's matching network*. The proposed method against load fluctuation represents a one-order *Wang's matching network*.

In conclusion, due to its special characteristics, *Wang's matching network* has great potential for development. The odd-order networks can improve ultrasonic system tolerance against load fluctuation, thus protecting the system. The even-order networks can keep the power factor at 1, and thereby improve the power transmission efficiency. Besides, high-order matching circuits have the function of increasing power output so that the output power grows exponentially with the order of n. In practice, the order should be selected based on the requirements and actual conditions.

IV. Experiments

A. Transducers Used in the Experiments

In the verification experiments, an ultrasonic cleaning transducer with the rated power of 100 W was used, and it is shown in Fig. 10(a). Before the experiments, it was installed under a cleaning sink, as shown in Fig. 10(b).

B. Ultrasonic Driving and Control System

An ultrasonic driving and control system was built to verify the proposed matching method. The system's schematic diagram of the system is shown in Fig. 11(a). A sinusoidal signal generated by a direct digital synthesis (DDS) chip was amplified by a class D power amplifier

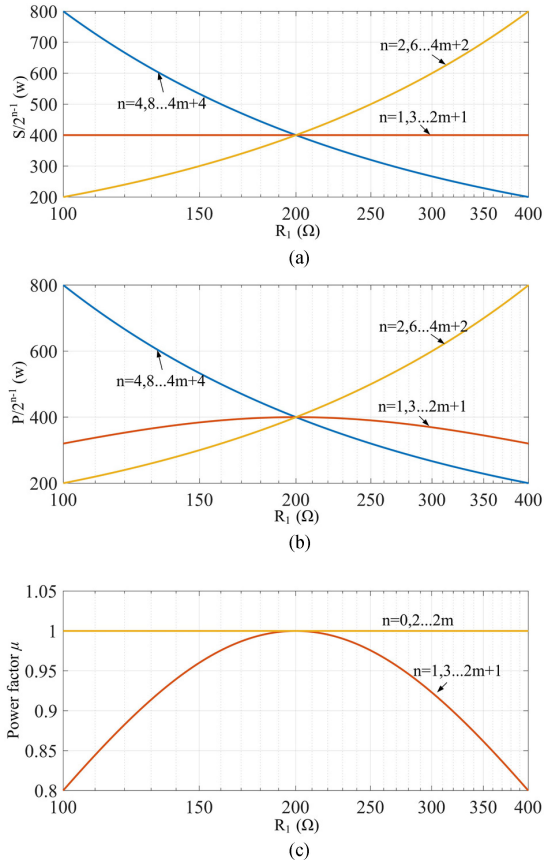

Fig. 9. Power$/2^{n-1}$-*load* curves (including S and P) and the *power factor-load* curves, with different n, of the proposed high-order matching circuit, where m are natural numbers. (a) Apparent power$/2^{n-1}$-*load* curves. (b) Active power$/2^{n-1}$-*load* curves. (c) Power factor-*load* curve.

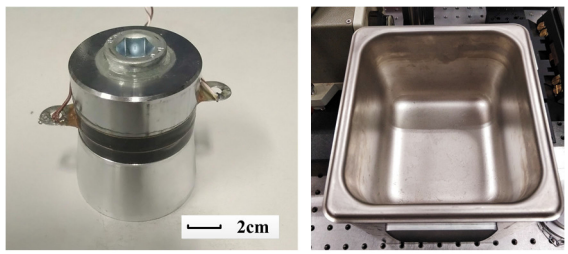

Fig. 10. (a) Transducer and (b) the cleaning sink used in the experiments.

to drive the transducer after matching. Unlike the traditional methods, we used two current sensors to collect two groups of current signals rather than collecting the voltage and current signals. One sensor was installed in the branch of the matching capacitor to sample current signal i_2, and the other one was installed in the branch of the transducer to sample current signal i_L. Then, i_2 and i_L were amplified and filtered by the signal processing circuit. Furthermore, the phase detection circuit and peak detection circuit detected the phase difference θ, and the peak values I_2 and I_L of i_2 and i_L, respectively. Signals I_2, I_L, and θ were gathered by an Advanced RISC Machine (ARM) microprocessor.

According to the equivalent circuit shown in Fig. 11(b), the voltage u across the transducer was expressed as follows:

$$u = \frac{i_2}{j\omega_{dr} C_2} = \frac{i_0}{j\omega_{dr} C_0}. \tag{43}$$

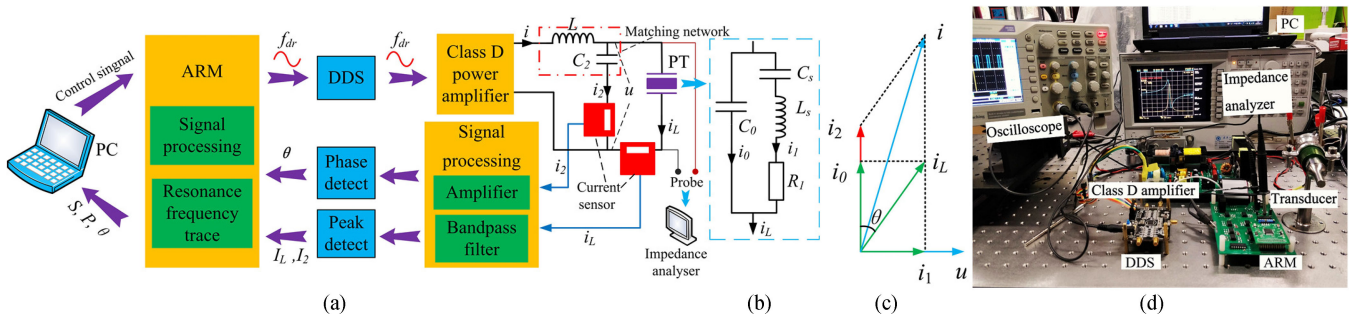

Fig. 11. Ultrasonic driving and control system. (a) System schematic diagram of the system. (b) Equivalent circuit of PT. (c) Vector diagram of the relevant parameters. (d) The physical experimental system.

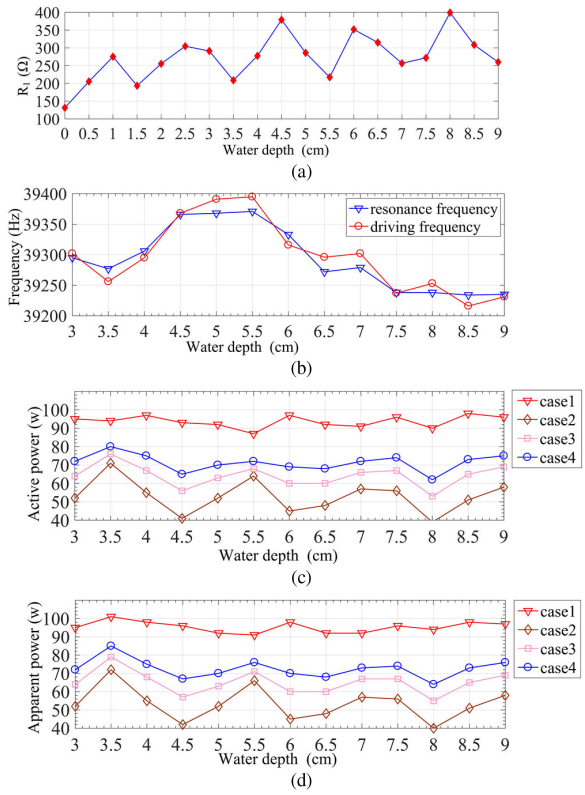

Fig. 12. Experimental results. (a) Change of R_1 over water depth. (b) Change of f_s over water depth and the driving frequency. (c) Apparent power S change curves over the water level under different cases. (d) Active power P change curves over the water level under different cases.

The current i_1 flowing through the series arm of the transducer was defined as follows:

$$i_1 = i_L - i_0 = i_L - i_2 C_0/C_2. \tag{44}$$

When f_{s2} was equal to the mechanical resonance frequency f_s, the series arm was pure resistance, and the phase of i_1 was the same as that of u. Defining the phase of u as zero, the vector diagram of the above variables was obtained, and it is illustrated in Fig. 11(b). According to Fig. 11(b), in the experiments, (44) could be expressed in a complex form as follows:

$$i_1 = I_L \sin\theta + j(I_L \cos\theta - I_2 C_0/C_2). \tag{45}$$

The total current *i* was expressed as follows:

$$i = i_L + i_2 = I_L \sin\theta + j(I_2 + I_L \cos\theta). \tag{46}$$

When the phase difference between i_1 and u was zero, the imaginary component M of i_1 should have been zero too, which is given by

$$M = I_L \cos\theta - I_2 C_0/C_2 = 0 \tag{47}$$

where M denoted the discriminant used in the RFT algorithm. After obtaining θ, I_2, and I_L, the ARM microprocessor will calculate the discriminant M in the following way.

1) When $-\Delta < M < \Delta$ (Δ was the given tolerance), the algorithm kept the driving frequency and terminated the searching process.
2) When $M > \Delta$, the series arm was capacitive, and thus the ARM controlled the DDS to decrease the driving frequency.
3) When $M < \Delta$, the series arm was inductive, and the ARM controlled the DDS to increase the driving frequency.

Using a classic algorithm, the binary search, based on the above processes, the RFT algorithm could track the mechanical resonance frequency f_s. Nonetheless, due to the unavoidable error in signal sampling, when Δ was set to a very small value, the algorithm could not converge. After carefully selecting through experiments, Δ was set to 0.012, and the search range was set from 38 to 42 kHz. When our developed system, shown in Fig. 11(d), was used, the RFT error was within $\pm$20 Hz.

Furthermore, the apparent power *S* and active power *P* were calculated by

$$S = |u| \cdot |i| = \frac{I_2}{\omega_{dr} C_2} \cdot \sqrt{(I_L \sin\theta)^2 + (I_2 + x I_L \cos\theta)^2}, \tag{48}$$

$$P = |u|\,|i| \cdot \cos\theta_{u,i} = |u|\,|i_1| = \frac{I_2}{\omega_{dr} C_2} \cdot I_L \sin\theta \tag{49}$$

where $\theta_{u,i}$ denoted the phase difference between *u* and *i*. Because the calculations were too complex, *S* and *P* were calculated in the top computer (PC).

C. Experimental Results and Discussion

The mechanical loss resistance R_1 of the ultrasonic cleaning transducer was closely associated with the water level, and the relationship between R_1 and the water level was not linear. Because of the effect of a standing wave, R_1 had an obvious cyclical fluctuation as the water level increased.

Water was slowly poured into the ultrasonic cleaning sink that is shown in Fig. 10(b). Note that when the water depth is less than 3 cm, the ultrasonic system cannot reach a stable state, thus we did not record data under 3 cm.

Furthermore, R_0 was set to 300 Ω. The driving voltage was set to 120 V. As measured by the impedance analyzer, R_1 varied within the range 200–400 Ω, as shown in Fig. 12(a), which represented the load fluctuation. The resonance frequency f_s varied in a 200 Hz range, as shown in Fig. 12(b); also, the RFT accuracy was higher than 25 Hz.

TABLE I
PARAMETERS OF DIFFERENT CASES

Parameters	Case1	Case2	Case3	Case4
Ideal ρ	$\sqrt{2}/2$	$1/4$	$1/2$	$1/\sqrt{3}$
Actual ρ	0.70	0.26	0.5	0.58

TABLE II
ANALYSIS RESULTS OF EXPERIMENTAL DATA

Parameters	Average value (W)		Mean square error (W)		Maximum fluctuation (W)	
	P	S	P	S	P	S
Case1	93.7	95.3	3.2	3.0	11	10
Case2	53	53.4	8.8	8.9	32	32
Case3	64.1	65	6.0	6.4	23	24
Case4	71.3	72.5	4.6	5.2	18	21

Driven by the ultrasonic driving and control system, the real-time apparent power and active power of the ultrasonic transducer were collected at every 0.5 cm for all the four cases, whose matching parameter ρ are listed in Table I. The actual matching parameters were slightly different from the ideal matching parameters. Fig. 12(c) and (d) show the power change with the increase in water depth in different cases. The values of relevant parameters after data processing are listed in Table II.

Table II shows that system performance was closely related to the matching parameter ρ. When $\rho = \sqrt{2}/2$, the system performed much better than in other cases. The experimental results were consistent with the simulation results. After matching by using the proposed method, there were still small fluctuations in the output power which was because of the environmental parameters change. However, the degree of these fluctuations was acceptable. In practice, the power fluctuation can severely weaken system performance, and reduce the machining quality. Besides, excessive power can even damage an ultrasonic system. The experimental results show that despite its simple structure the proposed matching method can address these problems well.

Compared with the closed-loop based methods and the adjustable components-based methods, there are only two components included in the proposed method. Thus, in terms of cost and implementation difficulty, the proposed method is much better than closed-loop-based methods and adjustable components-based methods. But apparently, our method is limited in a highly fluctuating environment that the absolute constant power cannot be achieved simply by using such a simple circuit. In high-performance scenarios, to achieve better constant power control, combining the proposed matching circuit and closed-loop control would be a good choice.

V. CONCLUSION

In this paper, a mathematical model has been developed to analyze the *LC* matching network for power ultrasonic transducer. A new parameter f_0 was defined to help solving the problem. And keeping the ultrasonic system's output power stable was considered as the primary design objective. According to the model, a high-tolerance matching method against load fluctuation was proposed, where the optimal value of f_{LC} is determined as $\sqrt{2}f_s$ ($\rho = \sqrt{2}/2$). The advantages and the sensitivity of the proposed method including the driving frequency error (Δf) and the matching frequency error (Δf_1) were analyzed in the simulations. The simulation results suggest that when $\rho = \sqrt{2}/2$ the transducer performs much better than the others, and the proposed matching method is still valid even if there are some environmental fluctuations and some error in RFT algorithms. And the experimental results show that the proposed matching method can indeed increase the system's tolerance of load fluctuation dramatically.

Owing to its simple structure and high performance, the proposed matching method can be widely applied in most ultrasonic systems, especially the power ultrasonic systems. For simple cost-effective systems, this method can be applied directly. For complex, high-performance ultrasonic systems, this method could be integrated with other solutions. While using closed-loop systems or adjustable components might make sense in specific systems, they cannot change the transducer's electrical properties radically. Although the proposed method cannot ensure absolute stability of the output, it can be used complementarily to improve the transducer's electrical properties and protect the system.

It is worth mentioning that the high-order matching circuits were also researched and a high-order matching circuit, denominated as *Wang's matching circuit*, was given, which may have much better application potential. When the driving frequency was fixed, the odd-order networks and the even-order networks could keep the apparent power and power factor constant no matter how the resistance changed. This special circuit can be used in other fields, and further research is still needed.

APPENDIX

See Table III.

TABLE III
VARIABLES INVOLVED AND THEIR MEANINGS

Variables	Meaning
C_0	Statistic Capacitor of PT
R_p	Dielectric loss resistance of PT
C_s	Dynamic capacitor of PT
R_1	Mechanical loss resistance of PT
L	Matching inductor
C	Matching capacitor
V_{in}	Voltage of driving signal
f_s (ω_s)	Mechanical resonance frequency
$f_{ma}(\omega_{ma})$	Frequency used in calculating matching parameters
$f_{dr}(\omega_{dr})$	Frequency of driving signal
f_{LC}	LC resonance frequency
R_0	Typical load resistance
ρ	Ratio of f_s to f_{LC}
ρ_1	Ratio of f_{ma} to f_s
ρ_2	Ratio of f_{dr} to f_s
ρ_3	Ratio of R_1 to R_0
Q_m	Mechanical quality factor
Z	Complex impedance of matched PT
$\lvert Z\rvert$	Impedance of matched PT
S	Apparent power
P	Active power
μ	Power factor
α_1	Ratio of actual S to typical S
α_2	Ratio of actual P to typical P
Δf	Driving frequency error (RFT error)
Δf_1	Matching frequency error
L_k	Inductance of the kth matching inductor
C_k	Capacitance of the kth matching capacitor
Z_n	Complex impedance of PT matched by n-order LC matching network
M	Discriminant in the RFT algorithm
Δ	Given tolerance in the RFT algorithm

REFERENCES

[1] G. Harvey, A. Gachagan, and T. Mutasa, "Review of high-power ultrasound-industrial applications and measurement methods," *IEEE Trans. Ultrason. Ferroelect. Freq. Control*, vol. 61, no. 3, pp. 481–495, Mar. 2014.

[2] F. Wang, H. Zhang, C. Liang, Y. Tian, X. Zhao, and D. Zhang, "Design of high-frequency ultrasonic transducers with flexure decoupling flanges for thermosonic bonding," *IEEE Trans. Ind. Electron.*, vol. 63, no. 4, pp. 2304–2312, Apr. 2016.

[3] Y. He *et al.*, "Ultrasonic power closed-loop control on wire bonder," in *Proc. 18th Electron. Packag. Technol. Conf.*, 2017, pp. 691–695.

[4] P. A. Juang and D. W. Gu, "Speed control of a new disc-type ultrasonic motor by using current controller," *IEEE Trans. Power Electron.*, vol. 21, no. 1, pp. 219–224, Jan. 2006.

[5] T. Senjyu, T. Kashiwagi, and K. Uezato, "Position control of ultrasonic motors using MRAC and dead-zone compensation with fuzzy inference," *IEEE Trans. Power Electron.*, vol. 17, no. 2, pp. 265–272, Mar. 2002.

[6] T. J. Mason, "Ultrasonic cleaning: An historical perspective," *Ultrason. Sonochem.*, vol. 29, pp. 519–523, 2016.

[7] X. Jiang, X. Zhang, X. Zhu, H. Sui, and D. Zhang, "Study of phase shift control in high-speed ultrasonic vibration cutting," *IEEE Trans. Ind. Electron.*, vol. 65, no. 3, pp. 2467–2474, Mar. 2018.

[8] X. Zhu, B. Lin, L. Liu, and Y. Luan, "Power transfer performance and cutting force effects of contactless energy transfer system for rotary ultrasonic grinding," *IEEE Trans. Ind. Electron.*, vol. 63, no. 5, pp. 2785–2795, May 2016.

[9] K. Ding, Y. Fu, H. Su, H. Xu, F. Cui, and Q. Li, "Experimental studies on matching performance of grinding and vibration parameters in ultrasonic assisted grinding of SiC ceramics," *Int. J. Adv. Manuf. Technol.*, vol. 88, nos. 9–12, pp. 2527–2535, 2017.

[10] T. B. Thoe, D. K. Aspinwall, and M. L. H. Wise, "Review on ultrasonic machining," *Int. J. Mach. Tools Manuf.*, vol. 38, no. 4, pp. 239–255, 1998.

[11] X. Li, P. Harkness, K. Worrall, R. Timoney, and M. Lucas, "A parametric study for the design of an optimized ultrasonic-percussive planetary drill tool," *IEEE Trans. Ultrason. Ferroelect. Freq. Control*, vol. 64, no. 3, pp. 577–589, Mar. 2017.

[12] S. Sherrit, H. D. Wiederick, B. K. Mukherjee, and M. Sayer, "An accurate equivalent circuit for the unloaded piezoelectric vibrator in the thickness mode," *J. Phys. D, Appl. Phys.*, vol. 30, no. 16, 1997, Art. no. 2354.

[13] H. Zhang, F. Wang, D. Zhang, L. Wang, Y. Hou, and X. Tao, "A new automatic resonance frequency tracking method for piezoelectric ultrasonic transducers used in thermosonic wire bonding," *Sens. Actuators A, Phys.*, vol. 235, pp. 140–150, 2015.

[14] A. Arnau, T. Sogorb, and Y. Jiménez, "A new method for continuous monitoring of series resonance frequency and simple determination of motional impedance parameters for loaded quartz-crystal resonators," *IEEE Trans. Ultrason. Ferroelect. Freq. Control*, vol. 48, no. 2, pp. 617–623, Mar. 2001.

[15] S. Ghenna, F. Giraud, C. Giraud-Audine, and M. Amberg, "Vector control of piezoelectric transducers and ultrasonic actuators," *IEEE Trans. Ind. Electron.*, vol. 65, no. 6, pp. 4880–4888, Jun. 2018.

[16] M. G. Kim, S. Yoon, H. H. Kim, and K. K. Shung, "Impedance matching network for high frequency ultrasonic transducer for cellular applications," *Ultrasonics*, vol. 65, pp. 258–267, 2016.

[17] Y. Yang, X. Wei, L. Zhang, and W. Yao, "The effect of electrical impedance matching on the electromechanical characteristics of sandwiched piezoelectric ultrasonic transducers," *Sensors*, vol. 17, no. 12, 2017, Art. no. E2832.

[18] M. Garcia-Rodriguez *et al.*, "Low cost matching network for ultrasonic transducers," *Phys. Procedia*, vol. 3, no. 1, pp. 1025–1031, 2010.

[19] L. Capineri, L. Masotti, M. Rinieri, and S. Rocchi, "Ultrasonic transducers as a black-box: Equivalent circuit synthesis and matching network design," *IEEE Trans. Ultrason. Ferroelect. Freq. Control*, vol. 40, no. 6, pp. 694–703, Nov. 1993.

[20] H. Carlin, "A new approach to gain-bandwidth problems," *IEEE Trans. Circuits Syst.*, vol. 24, no. 4, pp. 170–175, Apr. 1977.

[21] Y. C. Chen, S. Wu, and P. C. Chen, "The impedance-matching design and simulation on high power elctro-acoustical transducer," *Sens. Actuators A, Phys.*, vol. 115, no. 1, pp. 38–45, 2004.

[22] X. Jiang, X. Zhu, C. Y. Y. Wong, D. Zhang, and D. Geng, "Theory of series inductance matching to transducer at pre-mechanical resonance zone in ultrasonic vibration cutting," *IEEE Trans. Ind. Electron.*, vol. 66, no. 4, pp. 3019–3029, Apr. 2019.

[23] L. C. Cheng, Y. C. Kang, and C. L. Chen, "A resonance-frequency-tracing method for a current-fed piezoelectric transducer," *IEEE Trans. Ind. Electron.*, vol. 61, no. 11, pp. 6031–6040, Nov. 2014.

[24] Y. Kuang, Y. Jin, S. Cochran, and Z. Huang, "Resonance tracking and vibration stablilization for high power ultrasonic transducers," *Ultrasonics*, vol. 54, no. 1, pp. 187–194, 2014.

[25] H. J. Dong, J. Wu, G. Y. Zhang, and H. F. Wu, "An improved phase-locked loop method for automatic resonance frequency tracing based on static capacitance broadband compensation for a high-power ultrasonic transducer," *IEEE Trans. Ultrason. Ferroelect. Freq. Control*, vol. 59, no. 2, pp. 205–210, Feb. 2012.

[26] S. Lin, "Effect of electric load impedances on the performance of sandwich piezoelectric transducers," *IEEE Trans. Ultrason. Ferroelect. Freq. Control*, vol. 51, no. 10, pp. 1280–1286, Oct. 2004.

[27] Y. Kuang, M. R. Sadiq, S. Cochran, and Z. Huang, "Ultrasonic cutting with resonance tracking and vibration stabilization," in *Proc. IEEE Int. Ultrason. Symp.*, 2013, pp. 843–846.

[28] J. L. Pons, P. Ochoa, M. Villegas, J. F. Fernández, E. Rocon, and J. Moreno, "Self-tuned driving of piezoelectric actuators : The case of ultrasonic motors," *J. Eur. Ceram. Soc.*, vol. 27, no. 13, pp. 4163–4167, 2007.

[29] X. Liu, A. I. Colli-Menchi, J. Gilbert, D. A. Friedrichs, K. Malang, and E. Sánchez-Sinencio, "An automatic resonance tracking scheme with maximum power transfer for piezoelectric transducers," *IEEE Trans. Ind. Electron.*, vol. 62, no. 11, pp. 7136–7145, Nov. 2015.

[30] W. Shi, H. Zhao, J. Ma, and Y. Yao, "An optimum-frequency tracking scheme for ultrasonic motor," *IEEE Trans. Ind. Electron.*, vol. 64, no. 6, pp. 4413–4422, Jun. 2017.

[31] S. I. Furura, I. Maruhashi, and Nakaoka, "Load-adaptive frequency tracking control implementation of two-phase resonant inverter for ultrasonic motor," *IEEE Trans. Power Electron.*, vol. 7, no. 3, pp. 542–550, Jul. 1992.

[32] W. Feng, P. Mattavelli, and F. C. Lee, "Pulsewidth locked loop (PWLL) for automatic resonant frequency tracking in LLC DC–DC transformer (LLC-DCX)," *IEEE Trans. Power Electron.*, vol. 28, no. 4, pp. 1862–1869, Apr. 2013.

[33] H. Li and Z. Jiang, "On automatic resonant frequency tracking in LLC series resonant converter based on zero-current duration time of secondary diode," *IEEE Trans. Power Electron.*, vol. 31, no. 7, pp. 4956–4962, Jul. 2015.

[34] Z. Long, Z. Pan, C. Li, and J. Zhang, "Constant amplitude control of high-power ultrasonic drive system," in *Proc. IEEE Int. Conf. Inf. Autom.*, 2014, pp. 582–586.

[35] Y. Zao, Q. Ouyang, X. Zhang, S. Hou, and M. Fang, "The dynamic impedance matching method for high temperature electromagnetic acoustic transducer," in *Proc. Control Decis. Conf.*, 2017, pp. 1923–1927.

[36] Y. Lim, H. Tang, S. Lim, and J. Park, "An adaptive impedance-matching network based on a novel capacitor matrix for wireless power transfer," *IEEE Trans. Power Electron.*, vol. 29, no. 8, pp. 4403–4413, Aug. 2014.

[37] Y. Han and D. J. Perreault, "Analysis and design of high efficiency matching networks," *IEEE Trans. Power Electron.*, vol. 21, no. 5, pp. 1484–1491, Sep. 2006.

[38] A. Kumar, S. Sinha, A. Sepahvand, and K. Afridi, "Improved design optimization for high-efficiency matching networks," *IEEE Trans. Power Electron.*, vol. 33, no. 1, pp. 37–50, Jan. 2018.

[39] L. I. Xiaodong and A. K. S. Bhat, "Analysis and design of high-frequency isolated dual-bridge series resonant DC/DC converter," *IEEE Trans. Power Electron.*, vol. 25, no. 4, pp. 850–862, Apr. 2010.